



A model for the influence of steel corrosion products on nuclear fuel corrosion under permanent disposal conditions

L. Wu^a, Y. Beauregard^b, Z. Qin^a, S. Rohani^c, D.W. Shoesmith^{a,*}

^a Department of Chemistry, Western University, London, Ontario, Canada N6A 5B7

^b NOVA Chemicals Research and Technology Centre, 2928 16 Street, NE, Calgary, Alberta, Canada T2E 7K7

^c Department of Chemical and Biochemical Engineering, The University of Western Ontario, London, Ontario, Canada N6A 5B7

ARTICLE INFO

Article history:

Received 6 March 2012

Accepted 18 April 2012

Available online 25 April 2012

Keywords:

A. Steel

B. Modelling studies

C. Anodic dissolution

C. Interfaces

ABSTRACT

A model was developed to determine the influence of steel corrosion products on α -radiolytic corrosion of spent nuclear fuel inside a failed waste container. The model takes into account the α -radiolysis of water, the reaction of radiolytic H_2O_2 with UO_2 both directly and via galvanic coupling with noble metal particles, the reaction with H_2 via galvanic coupling, and the Fenton reaction. The dominant redox control agent was found to be H_2 , and the critical H_2 concentrations required to completely suppress fuel corrosion were calculated. The ability of Fe^{2+} to scavenge H_2O_2 had only a minor influence on fuel corrosion processes.

© 2012 Elsevier Ltd. All rights reserved.

1. Introduction

The recommended approach for the long term management of used nuclear fuel in Canada is adaptive phased management, and includes centralized containment and the isolation of the used fuel in a deep geological repository. As is common internationally, the Canadian repository concept is based on multiple barriers: the used fuel bundles, durable metal containers, a clay buffer and seals around the container, and a deep geologic environment [1]. A key barrier in this sequence is the container which model predictions suggest should sustain only minimal corrosion damage making failure unlikely [2].

It is judicious, however, to assume containers will fail, thereby, exposing the used fuel bundles to groundwater. While the Zircaloy cladding on the fuel is likely to provide an additional barrier to radionuclide release from the fuel, no credit is taken for this barrier for reasons documented elsewhere [1]. Since the groundwater entering the container will be anoxic, the only source of oxidants will be water radiolysis due to the radiation fields associated with the fuel. Under these conditions, fuel dissolution will be a corrosion reaction whose rate will evolve as radiation fields decay causing radiolytically-established redox conditions to change with time.

However, two corrosion fronts exist within the failed container: one on the fuel surface driven by radiolytic oxidants, and a second one on the carbon steel surface sustained by water reduction and producing the potential redox scavengers, Fe^{2+} and H_2 . Recent studies [3–5] show that a complex series of homogeneous solution and heterogeneous surface reactions will have a very significant influence on the redox conditions within the failed container and, hence, on the fuel corrosion/radionuclide release process.

Fig. 1 illustrates the redox coupling of the two corrosion fronts via the interactions of the radiolytic oxidant, H_2O_2 , and its potential decomposition product, O_2 , and the anoxic corrosion products, Fe^{2+} and H_2 . Fig. 2 shows the equilibrium potentials (E°) for the coupled anodic and cathodic reactions on each surface and the respective corrosion potentials (E_{CORR}) adopted by the fuel and the steel surfaces in the neutral to alkaline environment anticipated under disposal conditions [6–8]. The zone marked E_h indicates the redox condition expected due to the alpha radiolysis of water. The E_{CORR} zones indicate the range of corrosion potentials measured on fuel and steel electrodes. The redox gradient between the two corroding surfaces is clearly apparent.

In this paper a model is presented which attempts to calculate the influence of these reactions on fuel corrosion and the radionuclide release processes, although the latter is not discussed here. At its present stage of development the model is one dimensional and presumes the fuel surface is uniform. However, in the longer term the goal is to develop a model which will take into account the fractured nature of the spent fuel pellets and the geometry imposed by the Zircaloy cladding.

* Corresponding author. Tel.: +1 519 661 2111; fax: +1 519 661 3022.

E-mail address: dwshoesm@uwo.ca (D.W. Shoesmith).

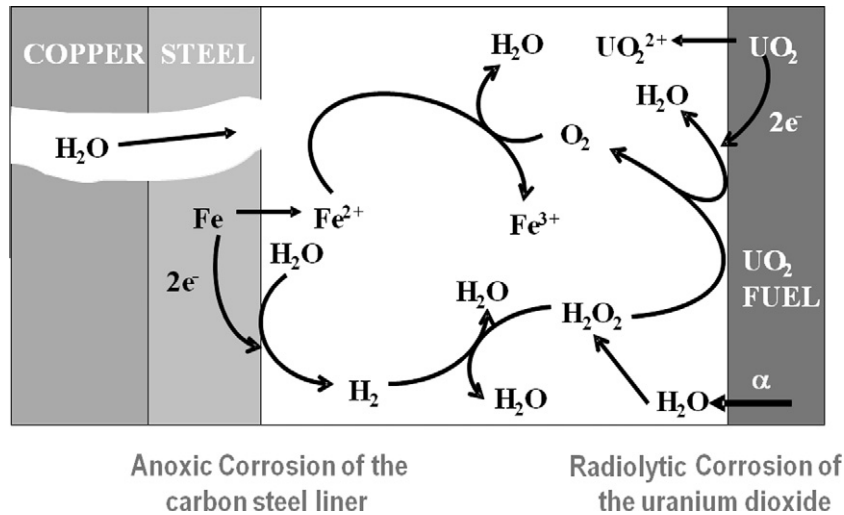


Fig. 1. Schematic showing the corrosion scenario inside a failed nuclear waste container.

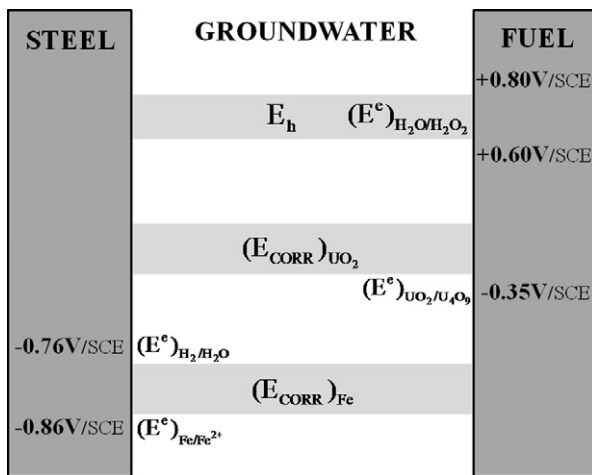


Fig. 2. Illustration showing the two corrosion fronts existing within a failed, groundwater flooded waste container, one on the fuel surface established by reaction with radiolytic oxidants and a second one on the steel surface established by reaction with water.

2. Model description

The rates of the various processes in the model are described by a series of one dimensional diffusion–reaction equations,

$$\frac{\partial c_i(x,t)}{\partial t} = D_i \frac{\partial^2 c_i(x,t)}{\partial x^2} + \sum_k R_k(i) \quad (1)$$

where $c_i(x,t)$ is the concentration of species i at point x and time t , D_i is the diffusion coefficient of species i , and $R_k(i)$ is the reaction rate of species i in reaction k . If i is a product in the reaction k , $R > 0$; on the other hand, if i is a reactant, $R < 0$. At steady state, Eq. (1) reduces to

$$D_i \frac{\partial^2 c_i(x)}{\partial x^2} = -\sum_k R_k(i) \quad (2)$$

suggesting a balance between the diffusion and reaction processes at steady state. The main reactions involved in the fuel and steel corrosion processes are schematically illustrated in Fig. 3.

The chemical properties of the fuel and the changes induced by in-reactor irradiation have been discussed elsewhere [3]. The fuel

can be considered to be a rare earth (RE^{III})-doped UO₂ matrix containing segregated noble metal particles (ϵ particles). Since the creation of RE^{III} at U^{IV} lattice locations induces holes in the U 5f band, in-reactor irradiation leads to an increase in matrix conductivity. Both the matrix conductivity and the number density of noble metal particles will increase with fuel burn-up, which can be measured either as the fraction of fuel atoms that underwent fission, e.g. 1.5at%, or as the energy released per mass of fuel metal, e.g. 220 MWh kgU⁻¹. From the corrosion perspective the fuel can be considered as a conductive and reactive matrix containing noble metal particles which could act as either cathodes or anodes depending on the prevailing solution redox conditions.

The only source of oxidants is the radiolysis of water, and of reductants, the anoxic corrosion of the steel. The model includes: (I) the generation of H₂O₂ by water radiolysis; (II) the oxidative dissolution (corrosion) of UO₂ supported by H₂O₂ reduction on both the UO₂ surface and noble metal particles; (III) the reduction of oxidized U species (U^V/U^{VI}) catalyzed by H₂ oxidation on noble metal particles; (IV) the scavenging of H₂O₂ in homogeneous solution by reaction with Fe²⁺; (V) the decomposition of H₂O₂ to O₂ and H₂O assumed to require catalysis by the UO₂ and noble metal particle (not shown in Fig. 3) surfaces. Presently, the steel corrosion reaction is not explicitly modelled but assumed to generate constant concentrations of Fe²⁺ and H₂. In practice these concentrations will be coupled by the overall stoichiometry of the steel corrosion process, but this is not presently incorporated into the model.

2.1. Water radiolysis

Since a reasonable assumption is that waste containers will remain unbreached over the period (of a few 100 years) [1] when γ/β radiation fields are significant, only α -radiolysis is considered as a source of oxidants. Among α -radiolysis products, only molecular oxidants are important since radical oxidants have short lifetimes and steady-state concentrations orders of magnitude lower than those of the molecular products [9]. Here, the only radiolytic oxidant considered is H₂O₂ which has been shown to be the dominant one [10].

The influence of H₂ on α -radiolysis is considerable but relatively unimportant for UO₂ dissolution when compared to the noble metal catalysis effect [11] (described below). Additionally, the radiolytic effect is effectively eliminated when ~ 1 mM of carbonate is present in the exposure solution. This can be attributed to the ability of HCO₃⁻ to scavenge radiolytically-produced OH[•] radicals,

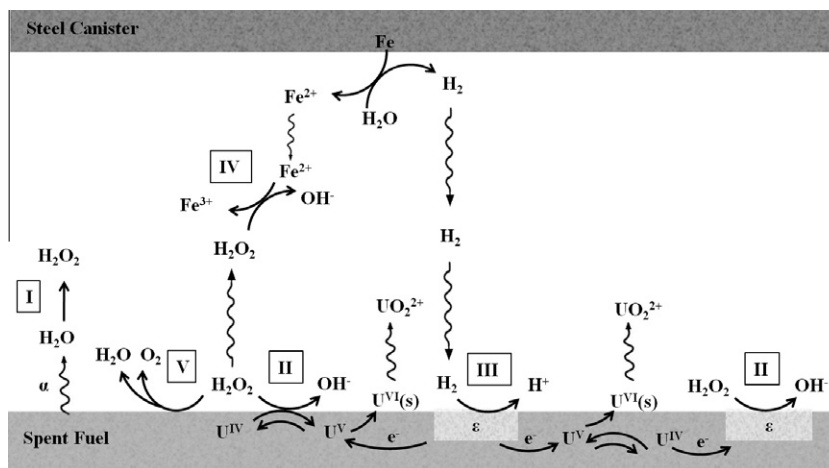


Fig. 3. Reactions considered in the model.



which prevents the reaction with H_2 to produce the reducing $\text{H} \cdot$ radical. Since $\text{CO}_3^{\cdot -}$ is a strong oxidant this facilitates oxidation while nullifying the H_2 effect. Since all groundwaters are likely to contain some carbonate, the influence of H_2 on α -radiolysis is therefore not included in this model.

Fig. 4 shows the fuel/groundwater interface, with x indicating the distance from the fuel surface. Since the dose rate for α -emitters in the fuel decreases with distance from the fuel surface, H_2O_2 will be produced with decreasing concentration over a range determined by the energy of specific α -particles [12]. In the model radiolysis is considered to occur uniformly within a thin layer of solution on the fuel surface with a thickness, b , given by the average penetration distance of α -radiation in water. Beyond this layer no H_2O_2 is produced. This approximation is taken for simplification, and the effect of non-uniform production of H_2O_2 is demonstrated to be marginal (Section 3.2). The diffusion layer is the distance over which species can diffuse to, or from, the fuel surface and beyond which uniform concentrations are presumed to prevail. Configured in this manner the model can be used to simulate small or large separations between the site of radiolytic H_2O_2 production (the fuel surface) and the source of potential scavengers, Fe^{2+} and H_2 (the steel surface).

The rate of H_2O_2 production is calculated using the expression,

$$R_{\text{H}_2\text{O}_2} = DR \cdot G_{\text{H}_2\text{O}_2} \cdot \rho_{\text{H}_2\text{O}} \quad (0 \leq x \leq b) \quad (4)$$

where DR is the dose rate representing the rate of the energy deposited per unit of mass, $G_{\text{H}_2\text{O}_2}$ is the radiolytic yield of H_2O_2 , which is

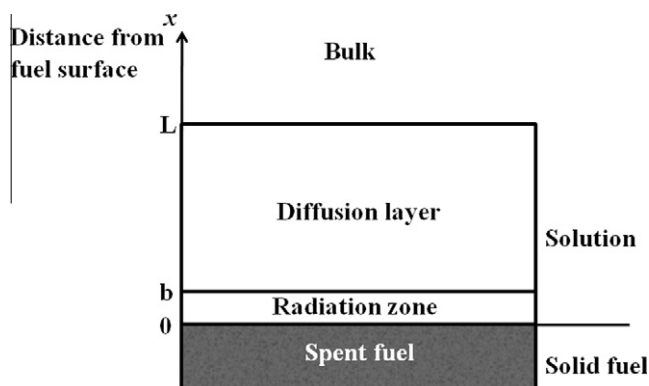


Fig. 4. One-dimensional α -radiolysis model.

the number of molecules produced per unit of radiation energy, and $\rho_{\text{H}_2\text{O}}$ is the density of water. The average alpha dose rate at the fuel surface for a burnup of 220 MWh kgU^{-1} at 1000 years is $9.03 \times 10^5 \text{ Gy a}^{-1}$ [13] and $G_{\text{H}_2\text{O}_2}$ is 1.13 mol J^{-1} [9].

2.2. UO_2 oxidation by H_2O_2

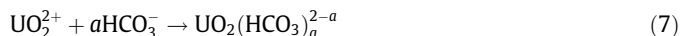
H_2O_2 can cause oxidation and dissolution (corrosion) of UO_2 via two reaction pathways [14,15] as illustrated in Fig. 3: (i) it can react directly with the UO_2 surface,



or, (ii) it can be reduced on noble metal particles leading to oxidation and corrosion by galvanic coupling to the UO_2 matrix. Irrespective of the location of the cathodic reaction, it would be expected to be first order with respect to $[\text{H}_2\text{O}_2]$ [10,16]

$$R_{\text{II}} = k_{\text{II}} \cdot [\text{H}_2\text{O}_2] \quad (x = 0) \quad (6)$$

Oxidation would proceed through the creation of a U^{V} intermediate prior to formation of U^{VI} and dissolution as UO_2^{2+} [6,17]. In carbonate-free solution this can lead to the formation of surface corrosion products ($\text{UO}_3 \cdot y\text{H}_2\text{O}$ or more complicated uranyl phases in groundwaters [17,18]) which would significantly influence the fuel dissolution rate [16]. In this model it is assumed that the location of dissolution is unimpeded in this manner, a situation which would exist in the presence of sufficient carbonate to completely complex the dissolution product [3],



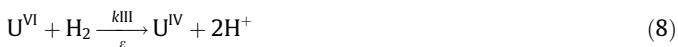
The experimental value for the rate constant, k_{II} , is $7.33 \times 10^{-8} \text{ m s}^{-1}$ on pure UO_2 [16]. This value was measured on UO_2 powder and hence may not be the appropriate value for spent fuel since the combination of noble metal particles and a rare earth-doped UO_2 matrix would be expected to accelerate the corrosion reaction via galvanic coupling. In the absence of a measured rate constant for this system a value of $7.33 \times 10^{-5} \text{ m s}^{-1}$ has been adopted. This value was used as an upper limit in simulations [19]. Some experimental evidence to justify such a high value will be presented below.

2.3. $\text{U}^{\text{V}}/\text{U}^{\text{VI}}$ reduction by H_2

A considerable effort has been expended on the study of the effect of H_2 on fuel corrosion since this reaction appears to have the potential to completely suppress corrosion and, hence,

radionuclide release [20,21]. Calculations indicate that dissolved H_2 concentrations as high as 0.038 mol/L [20] can be achieved as a consequence of steel corrosion in sealed repositories. The key requirement for H_2 to suppress fuel corrosion is that a mechanism to activate H_2 by dissociation to produce the H^\cdot radical species on the fuel surface be available. A range of studies have shown that this can be achieved by interaction of H_2 with both γ - and α -radiation and by catalysis on noble metal particles [20].

It has been experimentally demonstrated that the oxidation of the surface of simulated fuels (SIMFUELS which are both rare earth-doped and contain noble metal particles) can be suppressed in the presence of dissolved H_2 [3,22–24]. The primary mechanism for this suppression is the galvanic coupling of H_2 oxidation on noble metal particles to UO_{2+x} reduction on the fuel surface. While the details of this reaction remain unresolved, it is most likely that the oxidation/dissolution process is reversed at the U^V stage, as illustrated in Fig. 3 and described in detail elsewhere [24], and does not involve the reduction of dissolved UO_2^{2+} species. However, it has been shown that dissolution can commence as soon as oxidation of the UO_2 surface (to $U_{1-2x}^{IV}U_{2x}^V O_{2+x}$) begins [6] and occurs as UO_2^{2+} . To accommodate this feature in the model, it is assumed that a $U^{VI}(s)$ surface species is formed. At steady-state the surface coverage by this species will remain constant with the rate of release of U^{VI} to solution (as UO_2^{2+}) balanced by its rate of reformation by further oxidation of the $U_{1-2x}^{IV}U_{2x}^V O_{2+x}$ surface. Since it is assumed that the oxidation rate is rate determining, the surface coverage by $U^{VI}(s)$ will approach zero. In the model the overall reaction can be expressed as



The rate expression derived by Trummer et al. [25] for this reaction is,

$$R_{III} = k_{III} \cdot [H_2] \cdot s_\varepsilon \quad (x = 0) \quad (9)$$

where s_ε is the coverage of noble metal particles on the fuel surface, and the first-order rate constant k_{III} was measured to be $4 \times 10^{-7} \text{ m s}^{-1}$ for pellets containing 1at% Pd.

The value for the rate constant was measured on a UO_2 pellet containing 1at% Pd to simulate the presence of noble metal particles [25]. Since the UO_2 powder from which the pellet was made was nuclear grade, it is likely that the composition was close to stoichiometric. By comparison to a rare earth-doped SIMFUEL, the matrix conductivity would be low, and the range of galvanic coupling limited. Recent measurements of the resistivities of 1.5at% SIMFUEL (rare earth-doped) and a simulated fuel containing noble metal particles and not rare earth-doped showed that their resistivities are very different (182 ohm cm compared to 15,400 ohm cm, respectively [26]). As a consequence, the use of this rate constant could significantly underestimate the influence of galvanic coupling in its ability to suppress corrosion by catalyzing H_2 oxidation. It should be noted that the rate constants used for reactions (5) and (8) probably do not capture the correct balance between the ability of noble metal particles to catalyze reaction (5), which accelerates dissolution, and reaction (8) which suppresses it. This makes the use of the chosen value of k_{III} somewhat arbitrary.

Whether or not H_2 can react directly with the UO_2 surface remains unresolved. While Wren et al. [9] claimed that a $U_{1-2x}^{IV}U_{2x}^V O_{2+x}$ layer could catalyze the reaction between H_2O_2 and H_2 , thereby limiting the oxidation rate,



Nilsson and Jonsson [27] could find no evidence for this reaction. More recent results on a rare earth-doped SIMFUEL containing no noble metal particles suggested this reaction did occur

when the concentration ratio $[H_2]/[H_2O_2]$ was large, but the evidence was not totally convincing [28]. Irrespective of these uncertainties, the direct scavenging of H_2O_2 in this manner is unlikely to be kinetically competitive with this reaction on noble metal particles which is rapid but still considered to have only a small effect on the corrosion rate [29]. At present H_2O_2 scavenging in this manner, either by reaction on noble metal particles or on the UO_2 surface is not explicitly included in the model although its effect is implicitly included in experimental observations on SIMFUEL (see below).

It has also been claimed [30] that H_2 can reduce aqueous UO_2^{2+} to UO_2 via a homogeneous reaction:

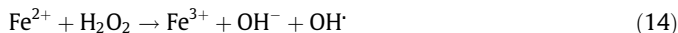


$$R'_{III} = k'_{III} \cdot [H_2] \cdot [UO_2^{2+}] \quad (0 \leq x \leq L) \quad (13)$$

This reaction is also built into the model although the second-order rate constant k'_{III} is fairly low ($3.6 \times 10^{-9} \text{ L mol}^{-1} \text{ s}^{-1}$). However, if this reaction is catalyzed by ε -particles, the reaction rate will increase significantly [27]. Although there is no reliable data at the low $[H_2]$ considered in this model, this aqueous phase reduction of $[UO_2^{2+}]$ by H_2 is not expected to affect spent fuel dissolution, and only lowers the concentration of radionuclides in solution. Hence, this catalyzed reduction of UO_2^{2+} by H_2 is not included in the present model.

2.4. Fenton reaction

Ferrous ions produced from the anoxic corrosion of the steel canister will undergo a homogeneous reaction with H_2O_2 in the Fenton reaction,



The overall rate constant with respect to $[Fe^{2+}]$ is k_{IV} [31]. Reaction (14) is the rate determining step and produces OH^\cdot radicals that can then react with Fe^{2+} or other potential reductants, such as H_2 and UO_2^{2+} . In the limiting case that reaction (15) is the only pathway for OH^\cdot consumption, the H_2O_2 reduction rate is given by

$$R_{IV}(H_2O_2) = \frac{1}{2}R_{IV}(Fe^{2+}) = -\frac{1}{2}k_{IV}[Fe^{2+}][H_2O_2] \quad (0 \leq x \leq L) \quad (16)$$

In the other limiting case where all the OH^\cdot radicals formed in reaction (14) are scavenged by alternative reaction pathways, Fe^{2+} oxidation occurs only via reaction (14) and the overall reaction rate of H_2O_2 consumption can be expressed as

$$R_{IV}(H_2O_2) = R_{IV}(Fe^{2+}) = -k_{IV}[Fe^{2+}][H_2O_2] \quad (0 \leq x \leq L) \quad (17)$$

In this model, the Fenton reaction is taken to be unimpeded by other reactions and the rate Eq. (16) is adopted. The rate constant, k_{IV} , has been shown to be very sensitive to pH, temperature and salinity [31]. Considering the long-term disposal conditions (e.g. saline groundwater, neutral pH ~ 9 , $\sim 25^\circ\text{C}$), a value of $1 \times 10^6 \text{ L mol}^{-1} \cdot \text{s}^{-1}$ is used for k_{IV} in this model [32–34].

2.5. H_2O_2 decomposition

The oxidation of H_2O_2 can couple to its reduction resulting in an overall decomposition to H_2O and O_2 ,



A number of studies claim to have observed this reaction on UO_2 [35–37] and an overall mechanism for H_2O_2 decomposition has been proposed [9]. Measurements of UO_2 dissolution and

H₂O₂ consumption rates showed that not all the H₂O₂ consumed caused dissolution suggesting decomposition [38]. An issue with most of these studies is that they were conducted at high [H₂O₂] (>10⁻⁴ mol L⁻¹) in solutions containing no carbonate and, hence, complicated by the formation of corrosion product deposits on the fuel surface. When carbonate was present and dissolution unimpeded by deposits [10,39], the discrepancy between UO₂²⁺ release and H₂O₂ consumption suggested ~20% of the H₂O₂ was not involved in the corrosion reaction; i.e., only 80% caused fuel dissolution.

In none of these studies was a quantitative kinetic analysis performed. Additionally, decomposition would be expected to be promoted by the presence of noble metal particles, but this has not been studied quantitatively. Given these uncertainties, we have assumed in the model that 20% of the H₂O₂ is consumed by decomposition. Since reaction (18) would produce the additional oxidant, O₂, which can also cause corrosion, some fraction of the decomposed H₂O₂ would still lead to fuel corrosion. However, the rate of reaction of O₂ with UO₂ is considerably slower than that of H₂O₂ [40] and this fraction is assumed in the model to be negligible. The adoption of a fraction of 20% can be considered conservative.

3. Model setup and results

The mathematical model outlined above is difficult to solve analytically, but numerical solutions can be developed using COMSOL Multiphysics, a commercial simulation package based on the finite element method. The model was simulated using the diluted species transportation module of COMSOL Multiphysics (version 4.2.0.150, COMSOL Inc.). The default values of the simulation parameters are listed in Table 1. A series of sensitivity analyses has been performed to examine the effects of diffusion length, [Fe²⁺], [H₂], and α-radiation dose rate, in which the parameters, other than those examined, were maintained at the default values.

3.1. The Influence of the diffusion length

As discussed above the diffusion layer is the distance over which species diffuse to or from the UO₂ surface. In the present form of the model this length could be taken to crudely represent either the depth of an inert-walled pore in a corrosion product deposit (μm), the distance from a flaw in the cladding (at which location the [H₂] remains undisturbed) to the site of H₂O₂ production

at a reactive surface location on the fuel (mm to cm), or the distance from the reactive fuel location to the site of H₂ production on the steel vessel wall (many cm).

Fig. 5 shows the simulated H₂O₂ concentration profiles as a function of diffusion length. The [H₂O₂] exhibits a maximum near the radiation penetration depth (0 < x < b), decreasing at locations closer to the surface due to its consumption by fuel corrosion and decreasing at larger distances along the diffusion path due to consumption in the Fenton reaction. The concentration reaches zero at the assumed diffusion length; i.e., at the boundary with the undisturbed bulk solution (x = L). Irrespective of the diffusion length, the great majority of the H₂O₂ is consumed within 0.2–0.3 mm of the corroding fuel surface.

The steady-state diffusive flux of UO₂²⁺ away from the UO₂ surface is equal to the fuel corrosion rate. As shown in Fig. 6, the flux (corrosion rate) only increases by a factor of ~2 as the diffusion length increases by three orders of magnitude, and is nearly independent of diffusion length for L > 0.1 mm. Thus, the effect of diffusion length on the fuel corrosion is marginal.

3.2. The effect of non-uniform dose rate distribution

In the present model, the dose rate is assumed to be uniformly distributed within a radiation zone near the fuel/water interface (x ≤ b) and to be zero in the solution beyond this region (x > b). However, the dose rate will actually be non-uniformly distributed since the α-particles will lose energy along the penetration pathway. Therefore, the use of this simplified uniform distribution should be tested.

The dose rate distribution in water in contact with used fuels has been studied using different approaches. One approach is based on the thermal power of the fuel and the ratio between the specific stopping power values in water and in UO₂ [13,41,42]. Another approach takes the geometrical consideration of radiation emitters and energy deposition into account, and simulations have been performed on spherical [43] and planar [12] geometries for spent fuel. Despite the different approaches, good agreement is achieved between the two calculations [43]. Here, we compare the results using the uniform dose rate distribution with the geometrical distribution obtained in Ref. [12].

Nielsen and Jonsson [12] calculated the dose rate by dividing the fuel matrix (α-radiation emitter) into thin layers at different depths from the surface using a planar geometry assumption. The maximum distance that α-particles can travel in UO₂ is

Table 1
Default values of simulation parameters.

Parameter	Symbol	Value	Units
Diffusion layer depth	L	1 × 10 ⁻³	m
Radiation zone depth [13]	b	1.3 × 10 ⁻⁵	m
Average α dose rate [13]	DR	9.03 × 10 ⁵	Gy a ⁻¹
H ₂ O ₂ radiolytic yield [9]	G _{H₂O₂}	1.13	mol J ⁻¹
H ₂ O ₂ diffusivity [9]	D _{H₂O₂}	1 × 10 ⁻⁹	m ² s ⁻¹
UO ₂ ²⁺ diffusivity [9]	D _{UO₂²⁺}	1 × 10 ⁻⁹	m ² s ⁻¹
H ₂ diffusivity [9]	D _{H₂}	5.85 × 10 ⁻⁹	m ² s ⁻¹
Fe ²⁺ diffusivity	D _{Fe}	1 × 10 ⁻⁹	m ² s ⁻¹
H ₂ O ₂ bulk concentration	C _{H₂O₂bulk}	0	mol L ⁻¹
H ₂ bulk concentration	C _{H₂bulk}	1 × 10 ⁻⁶	mol L ⁻¹
Fe ²⁺ bulk concentration [47]	C _{Fe-bulk}	1 × 10 ⁻⁶	mol L ⁻¹
ε-particle coverage [11]	S _ε	0.01	–
H ₂ O ₂ surf. reaction rate const. [19]	k _{II}	7.33 × 10 ⁻⁵	m s ⁻¹
H ₂ surf. reaction rate const. [25]	k _{III}	4 × 10 ⁻⁷	m s ⁻¹
H ₂ /UO ₂ ²⁺ bulk reaction rate const. [30]	k' _{III}	3.6 × 10 ⁻⁹	L mol ⁻¹ s ⁻¹
Fe ²⁺ bulk reaction rate const. [31]	k _{IV}	1 × 10 ⁶	L mol ⁻¹ s ⁻¹
H ₂ O ₂ decomposition ratio [39]	Ratio	0.2	–

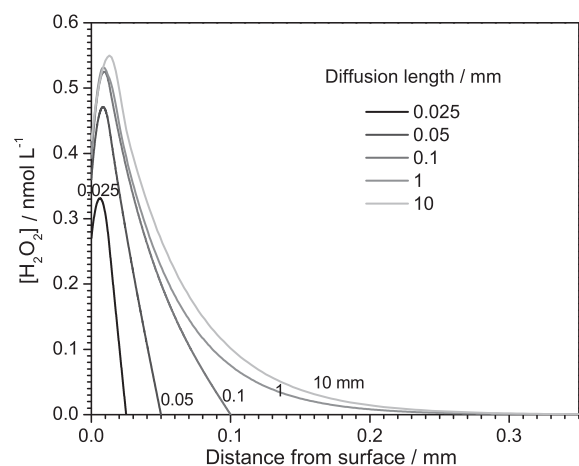


Fig. 5. H₂O₂ steady-state concentration profiles for various assumed diffusion lengths.

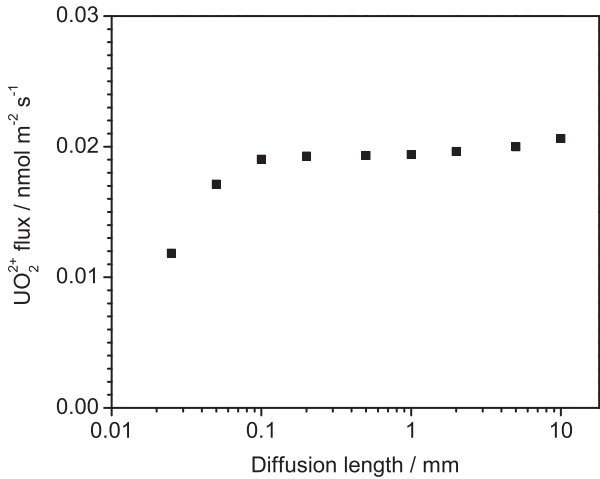


Fig. 6. Diffusive fluxes of UO_2^{2+} (equal to the UO_2 corrosion rate) as a function of various diffusion lengths.

$\sim 13 \mu\text{m}$; thus, only emitters located near the fuel surface contribute to solution radiolysis. The α -particles able to escape from the surface have a reduced energy after travelling through the fuel matrix. By integrating all contributions, the dose rate was obtained as a function of distance into the solution.

The calculated α -dose rate profile shows a sharp decrease with distance from the surface. Although this result is not specific for CANDU fuel, the authors conclude that fuels of different burnup and age will have the same profile of geometrical dose distribution which only differs in magnitude. It is found that their profile can be well fitted by an exponential function,

$$D(x) = A \left[\exp\left(-\frac{x}{B}\right) + C \right] \quad (x \leq \delta) \quad (19)$$

where A , the magnitude of the curve, depends on the burnup and age of the fuel, B , which determines the shape of the curve and remains the same between different fuels, and C is a constant that assures the dose rate reaches zero at the maximum penetration depth δ .

The fitted curve for the dose rate distribution is plotted in Fig. 7, yielding the values $A = 0.563 \text{ Gy s}^{-1}$, $B = 12.97 \mu\text{m}$ and $C = -0.0657$. The value of A needs to be adjusted to make the total dose rate consistent for both a uniform and an exponential distribution, i.e., a value for A that yields an area under the curve $D(x)$ equal to that under the line DR is required, Fig. 8.

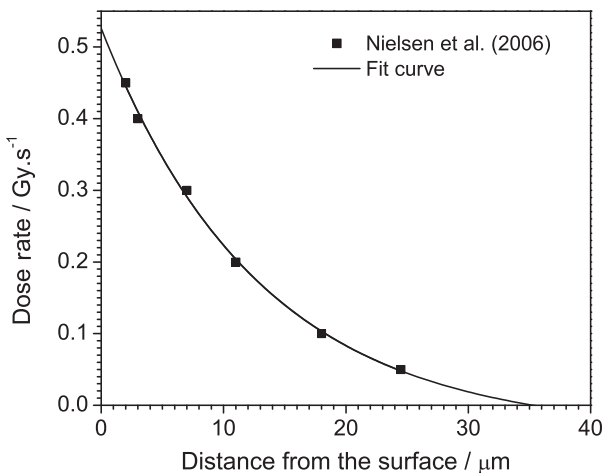


Fig. 7. Fitting results for the α -dose rate profile, using the data from Ref. [12].

For the total dose rates from each distribution to be equal,

$$\int_{x=0}^{\delta} D(x) dx = DR \cdot b \quad (20)$$

where the maximum penetration depth δ of α -particles in water is calculated to be $35.3 \mu\text{m}$ according to the fitting result. Using $DR = 9.03 \times 10^5 \text{ Gy a}^{-1}$ and $b = 13 \mu\text{m}$ [13], the value of A is calculated to be $2.30 \times 10^6 \text{ Gy a}^{-1}$. Therefore the exponential distribution of dose rate can be expressed as a function of distance

$$D(x) = 2.3 \times 10^6 \times \left[\exp\left(-\frac{x}{12.97}\right) - 0.0657 \right] \quad (\text{Gy}\cdot\text{a}^{-1}) \quad (0 \leq x \leq 35.3 \mu\text{m}) \quad (21)$$

As a comparison the uniform distribution is given by

$$D(x) = DR = 9.03 \times 10^5 \quad (\text{Gy}\cdot\text{a}^{-1}) \quad (0 \leq x \leq 13 \mu\text{m}) \quad (22)$$

Fig. 9 shows a comparison of the steady-state $[\text{H}_2\text{O}_2]$ profiles calculated based on either the uniform or exponential dose distribution. The position of the peak shifts to higher values of x , except for $L = 0.025 \text{ mm}$, and the peak values for $[\text{H}_2\text{O}_2]$ appear lower when using an exponential distribution. These profiles reflect the balance between the various consumption pathways for H_2O_2 , including UO_2 oxidation, the Fenton reaction and mass transport.

The influence of dose rate distributions on the UO_2^{2+} fluxes (corrosion rates) is shown in Fig. 10. The differences for the two distributions are marginal for varying diffusion lengths. Moreover, the results for a uniform distribution are slightly higher than those for an exponential distribution, suggesting that the former is a conservative approach. Based on this comparison the use of a simplified uniform distribution is justified.

3.3. The Influence of $[\text{Fe}^{2+}]$

The Fenton reaction will consume H_2O_2 in solution and would be expected to suppress the corrosion rate. Fig. 11 shows the influence of $[\text{Fe}^{2+}]$ on the $[\text{H}_2\text{O}_2]$ distribution profile for $[\text{Fe}^{2+}]_{\text{bulk}}$ up to $10^{-6} \text{ mol L}^{-1}$. For groundwaters with a pH in the expected range of 8–10, the solubility of Fe^{2+} will be in the range 10^{-4} – $10^{-6} \text{ mol L}^{-1}$ [44]. In the absence of Fe^{2+} , and beyond the range of influence of the corroding surface, there is a constant flux of H_2O_2 to the bulk of solution. As $[\text{Fe}^{2+}]_{\text{bulk}}$ is increased, H_2O_2 is scavenged by the Fenton reaction at locations progressively closer to the UO_2 surface. For $[\text{Fe}^{2+}]_{\text{bulk}} \geq 10^{-6} \text{ mol L}^{-1}$, the H_2O_2 is effectively totally consumed for distances from the fuel surface $> 0.2 \text{ mm}$.

At the fuel surface the influence of Fe^{2+} will be determined by the relative rates of the corrosion and Fenton reactions. As shown in Fig. 12, the Fenton reaction is able to influence the corrosion

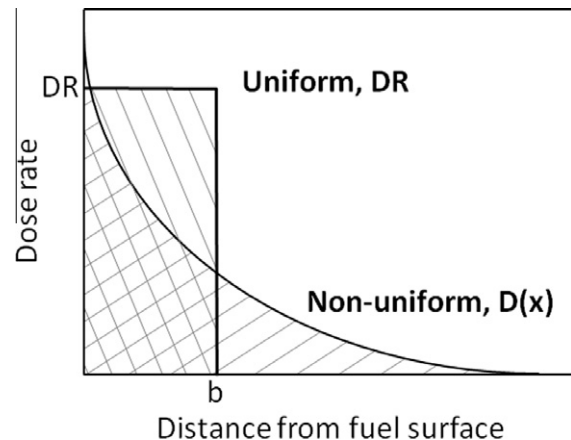


Fig. 8. Illustration showing the two different dose rate distributions; uniform and exponential. The shaded areas indicate the total dose rate in each case.

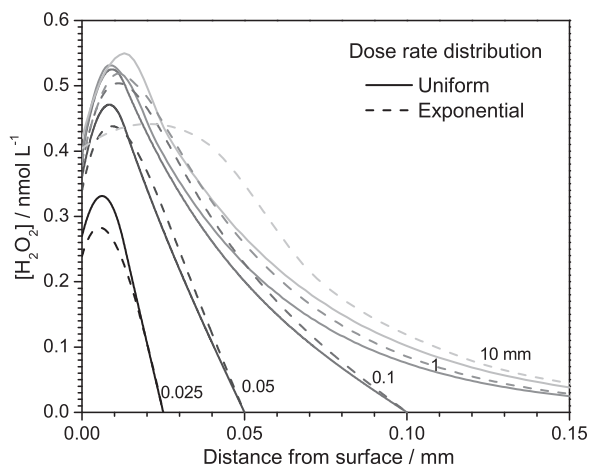


Fig. 9. H_2O_2 steady-state concentration profiles for both uniform and exponential dose rate distributions.

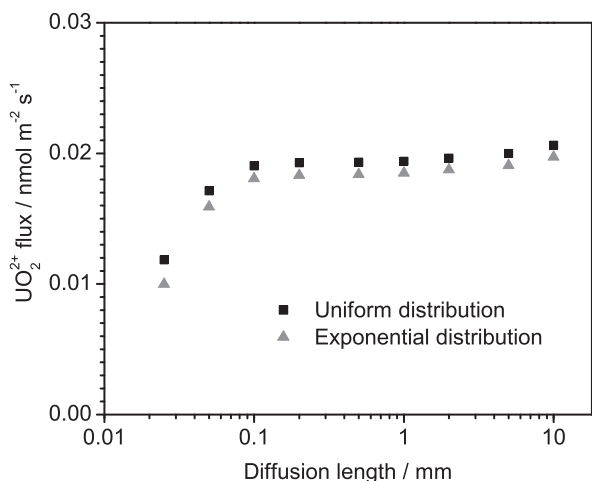


Fig. 10. Diffusive fluxes of UO_2^{2+} calculated for the two dose rate distributions. (\blacktriangle) exponential distribution; (\blacksquare) uniform distribution.

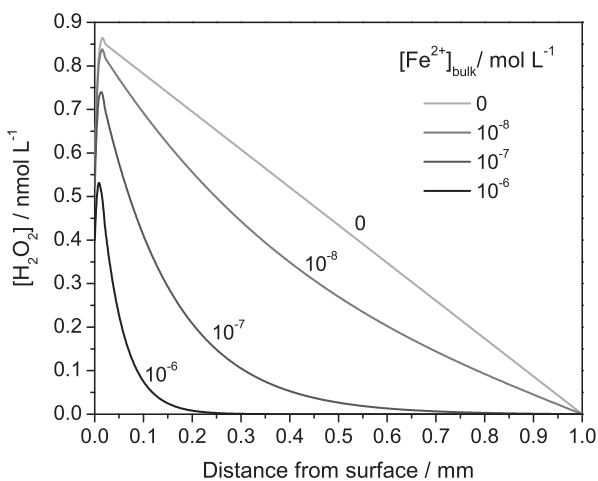


Fig. 11. $[\text{H}_2\text{O}_2]$ as a function of distance from fuel surface at various Fe^{2+} bulk concentrations.

process, leading to a decrease in flux of UO_2^{2+} as the H_2O_2 is consumed and corrosion suppressed. However, this influence is relatively minor, the corrosion rate (flux of UO_2^{2+}) being reduced by

only a factor of ~ 2 for an increase in $[\text{Fe}^{2+}]$ from 10^{-8} to 10^{-6} mol L^{-1} . Clearly, a $[\text{Fe}^{2+}]_{\text{bulk}}$ approaching the solubility limit would be required before any significant influence of the Fenton reaction on fuel corrosion would be observed.

3.4. The Influence of H_2

Fig. 13 shows the UO_2^{2+} flux (corrosion rate) as a function of bulk $[\text{H}_2]$ over the range 0 to $>10^{-5}$ mol L^{-1} . A linear relationship is obtained. Its extrapolation to zero fuel corrosion rate predicts the threshold $[\text{H}_2]$ at which the rate of UO_2 oxidation by H_2O_2 is balanced by the rate of its subsequent reduction by H_2 . This concentration can be considered the critical value, $[\text{H}_2]_{\text{crit}}$, at which fuel corrosion becomes completely suppressed. Based on this extrapolation, a value of $[\text{H}_2]_{\text{crit}} = 5.9 \times 10^{-6}$ mol L^{-1} was obtained.

This value is considerably higher than those calculated by Trummer and Jonsson [11]. This is a direct consequence of adopting a large value for k_{II} , the rate constant for the reaction of H_2O_2 with the UO_2 surface, reaction (5). In the absence of a value for k_{II} measured on noble metal-containing, rare earth-doped UO_2 (e.g., SIMFUEL) our value (Table 1) is somewhat arbitrarily chosen. Considering the magnitude and potential significance of this H_2 effect some justification confirming the magnitude is required. Two SIMFUEL experiments are considered here.

In the first experiment [22], the corrosion potential (E_{CORR}) of a 1.5at% SIMFUEL electrode was measured in 0.1 mol L^{-1} KCl (pH = 9.5; 60 °C) as the overpressure of a 5% H_2/Ar purge gas was steadily increased. The E_{CORR} decreased as the overpressure was increased. The thermodynamic threshold for the onset of UO_2 oxidation is around -350 mV (vs Ag/AgCl) and it has been verified experimentally by a combination of electrochemistry and X-ray photoelectron spectroscopy (XPS) [3,18] that oxidation below this value is undetectable. Consequently, the $[\text{H}_2]$ required to suppress E_{CORR} to ≤ -350 mV (vs Ag/AgCl) can be considered as the critical value, $[\text{H}_2]_{\text{crit}}$, required to prevent corrosion when galvanic coupling is present and H_2 oxidation is sustained on noble metal particles [22]. Using the solubility of H_2 [45] and the fact that this solubility is proportional to the partial pressure of H_2 [46], $[\text{H}_2]_{\text{crit}}$ can be calculated to be $\sim 1.8 \times 10^{-5}$ mol L^{-1} , which is compatible with the calculated model value of 5.9×10^{-6} mol L^{-1} .

In the second experiment [24] the ability of H_2 to prevent (or reverse) the oxidation of UO_2 was followed by measuring E_{CORR} on 1.5at% SIMFUEL when various concentrations of H_2O_2 were added to a 5% H_2/Ar -purged 0.1 mol L^{-1} KCl solution (pH = 9.5; 60 °C). In these experiments a concentration of dissolved H_2 of

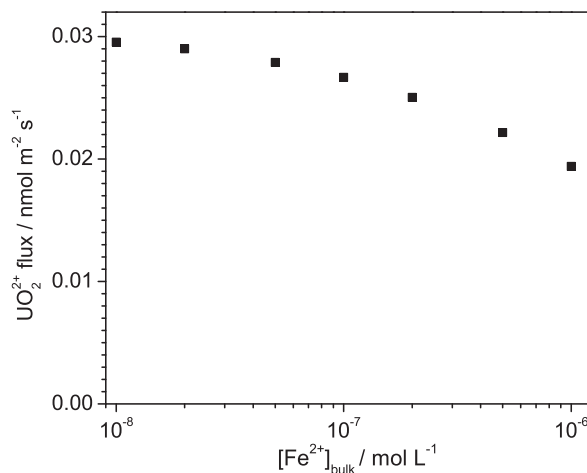


Fig. 12. UO_2^{2+} flux (equal to the UO_2 corrosion rate) as a function of $[\text{Fe}^{2+}]$.

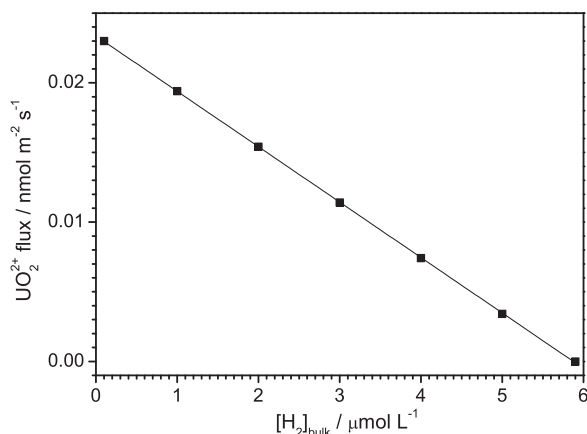


Fig. 13. UO_2^{2+} flux (equal to the UO_2 corrosion rate) as a function of $[\text{H}_2]_{\text{bulk}}$.

$\sim 3 \times 10^{-5} \text{ mol L}^{-1}$ was able to suppress E_{CORR} to the thermodynamic limit for a $[\text{H}_2\text{O}_2]$ up to 10^{-10} – $10^{-9} \text{ mol L}^{-1}$. That oxidation of the UO_2 surface was prevented when this E_{CORR} value was established was demonstrated by XPS. Since the calculated $[\text{H}_2\text{O}_2]$ s for the model are within the range of concentrations used in this experiment, $3 \times 10^{-5} \text{ mol L}^{-1}$ can be considered as a reasonable estimate of $[\text{H}_2]_{\text{crit}}$, which is compatible with the model value of $5.9 \times 10^{-6} \text{ mol L}^{-1}$. Based on the agreement between these experimental values and the model calculations, the adoption of the value of k_{II} (Table 1) seems reasonable.

3.5. Influence of α -radiation dose rate

Using the α -dose rates for an aged CANDU fuel bundle with a burnup of 220 MWh kgU^{-1} [13], values of $[\text{H}_2]_{\text{crit}}$ for different waste disposal times can be calculated. Fig. 14 shows the H_2 required to completely suppress fuel corrosion as a function of disposal time. As expected this calculation demonstrates that the H_2 requirement (demand) decreases markedly with time as α -radiation fields decay.

The increase in H_2 demand at short times is attributed to the ingrowth of α -emitters as a consequence of the short term decay of γ/β -radiation fields emitted by the fuel but not considered here. This raises the question as to whether the H_2 demand would be substantially increased in the improbable event of the fuel being exposed to groundwater during the early period when γ/β fields are significant. This seems highly unlikely since H_2 is commonly

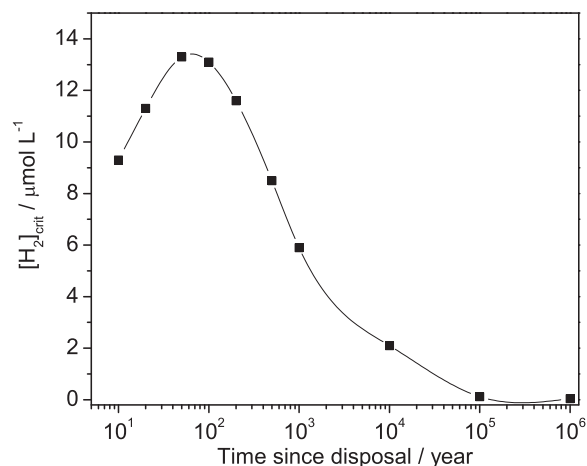


Fig. 14. Critical $[\text{H}_2]$ required to completely suppress fuel corrosion as a function of waste disposal time.

added to nuclear reactor heat transport circuits to suppress the radiolysis of water. Additionally, studies on spent fuel corrosion when γ/β fields are substantial show a very clear suppression of fuel corrosion and radionuclide release in the presence of dissolved H_2 [20].

4. Future requirements and model development

In its present form the model should be considered preliminary, and containing some rate constants whose values should be considered somewhat arbitrary. A considerable improvement in the available data base will be required before more justifiable predictions can be computed. Of particular importance is an improved quantitative kinetic understanding of the combined effects of RE^{III} doping and the number density of noble metal particles on H_2O_2 reduction and decomposition, H_2 oxidation, and the anodic reactivity of the UO_2 matrix.

The incorporation of a model for steel corrosion is also required. This model would need to couple the concentrations of H_2 and Fe^{2+} , and also to include the possibility that the rate of corrosion could be modified by the influence of the products of H_2O radiolysis and fuel dissolution (UO_2^{2+}). Although the calculations presented in this paper appear to indicate that the Fenton reaction would rule out the transport of H_2O_2 to oxidize, and potentially passivate the steel surface, there is no similar restraint on the transport of the potential oxidant, UO_2^{2+} to the steel surface. While the evidence to determine whether the accumulation of U, either absorbed as U^{VI} or deposited as reduced U^{IV} , is presently unavailable, it is likely these processes will influence the overall fuel corrosion rate. Similarly, the accumulation of Fe^{III} corrosion product deposits on the UO_2 surface could also influence the fuel corrosion rate.

A primary goal of this model is to determine how the physical properties of the fuel and the geometry of the fuel cladding with respect to its failure influence the interaction of the two corrosion fronts. Of particular importance is the need to assess the efficiency of H_2 in suppressing fuel corrosion at locations within fractures in fuel pellets or within locally failed fuel bundles when the transport access of hydrogen is limited and the available surface area of corroding fuel large. This will require the extension of the model to include two dimensional processes and should be achievable using COMSOL procedures.

5. Summary and conclusions

A model has been developed to determine the influence of steel corrosion products on the α -radiolytic corrosion of spent fuel. The model takes into account the α -radiolysis of water, the reaction of radiolytic H_2O_2 with UO_2 both directly and via galvanic coupling with noble metal particles, the reaction with H_2 via galvanic coupling, and the Fenton reaction. The direct influence of H_2 on the production of H_2O_2 by α -radiolysis is not included. The dominant redox control agent was found to be H_2 . The ability of Fe^{2+} to scavenge H_2O_2 by the Fenton reaction has only a minor influence on the fuel corrosion process. Critical H_2 concentrations, the $[\text{H}_2]$ required to completely suppress fuel corrosion, were calculated as a function of α -dose rate for various spent fuel ages. Even for the highest α -dose rates (anticipated after ~ 100 years of disposal) $[\text{H}_2]_{\text{crit}}$ was $\leq 1.5 \times 10^{-5} \text{ mol L}^{-1}$.

Acknowledgements

This research was funded under the Industrial Research Chair agreement between the Natural Science and Engineering Research Council (NSERC, Ottawa) and the Nuclear Waste Management Organization (NWMO, Toronto).

References

- [1] J. McMurry, D.A. Dixon, J.D. Garroni, B.M. Ikeda, S. Stroes-Gascoyne, P. Baumgartner, T.W. Melnyk, Evolution of a Canadian Deep Geologic Repository: Base Scenario, Report O6819-REP-01200-10092-R00, Ontario Power Generation, Toronto, ON, 2003.
- [2] F. King, M. Kolar, The Copper Container Corrosion Model Used in AECL's Second Case Study, Report O6819-REP-01200-10041-R00, Ontario Power Generation, Toronto, 2000.
- [3] D.W. Shoesmith, Used Fuel and Uranium Dioxide Dissolution Studies – A Review, Report NWMO TR-2007-03, Nuclear Waste Management Organization, Toronto, ON, 2007.
- [4] D.W. Shoesmith, The Role of Dissolved Hydrogen on the Corrosion/Dissolution of Spent Nuclear Fuel, Report NWMO TR-2008-19, Nuclear Waste Management Organization, Toronto, ON, 2008.
- [5] G.M. Kwong, Status of Corrosion Studies for Copper Used Fuel Containers Under Low Salinity Conditions, Report NWMO TR-2011-14, Nuclear Waste Management Organization, Toronto, ON, 2011.
- [6] D.W. Shoesmith, Fuel corrosion waste process under waste disposal conditions, *J. Nucl. Mater.* 282 (2000) 1–31.
- [7] C.T. Lee, M.S. Odziemkowski, D.W. Shoesmith, An in situ Raman-electrochemical investigation of carbon steel corrosion in $\text{Na}_2\text{CO}_3/\text{NaHCO}_3$, Na_2SO_4 , and NaCl solutions, *J. Electrochem. Soc.* 153 (2006) B33–B41.
- [8] C.T. Lee, Z. Qin, M.S. Odziemkowski, D.W. Shoesmith, The influence of groundwater anions on the impedance behaviour of carbon steel corroding under anoxic conditions, *Electrochim. Acta* 51 (2006) 1558–1568.
- [9] J.C. Wren, D.W. Shoesmith, S. Sunder, Corrosion behavior of uranium dioxide in alpha radiolytically decomposed water, *J. Electrochem. Soc.* 152 (2005) B470.
- [10] E. Ekeröth, O. Roth, M. Jonsson, The relative impact of radiolysis products in radiation induced oxidative dissolution of UO_2 , *J. Nucl. Mater.* 355 (2006) 38–46.
- [11] M. Trummer, M. Jonsson, Resolving the H_2 effect on radiation induced dissolution of UO_2 -based spent nuclear fuel, *J. Nucl. Mater.* 396 (2010) 163–169.
- [12] F. Nielsen, M. Jonsson, Geometrical α - and β -dose distributions and production rates of radiolysis products in water in contact with spent nuclear fuel, *J. Nucl. Mater.* 359 (2006) 1–7.
- [13] F. Garisto, D.H. Barber, E. Chen, A. Inglot, C.A. Morrison, Alpha, Beta and Gamma Dose Rates in Water in Contact with Used CANDU Fuel, Report NWMO TR-2009-27, Nuclear Waste Management Organization, Toronto, ON, 2009.
- [14] J.S. Goldik, J.J. Noël, D.W. Shoesmith, The electrochemical reduction of hydrogen peroxide on uranium dioxide electrodes in alkaline solution, *J. Electroanal. Chem.* 582 (2005) 241–248.
- [15] J.S. Goldik, J.J. Noël, D.W. Shoesmith, The effects of simulated fission products in the reduction of hydrogen peroxide on simulated nuclear fuel electrodes, *J. Electrochem. Soc.* 153 (2006) E151–E159.
- [16] M. Hossain, E. Ekeröth, M. Jonsson, Effects of HCO_3^- on the kinetics of UO_2 oxidation by H_2O_2 , *J. Nucl. Mater.* 358 (2006) 202–208.
- [17] B.G. Santos, J.J. Noël, D.W. Shoesmith, The effect of pH on the anodic dissolution of SIMFUEL (UO_2), *J. Electroanal. Chem.* 586 (2006) 1–11.
- [18] B.G. Santos, H.W. Nesbitt, J.J. Noël, D.W. Shoesmith, X-ray photoelectron spectroscopy study of anodically oxidized SIMFUEL surfaces, *Electrochim. Acta* 49 (2004) 1863–1873.
- [19] F. Nielsen, M. Jonsson, Simulations of H_2O_2 concentration profiles in the water surrounding spent nuclear fuel taking mixed radiation fields and bulk reactions into account, *J. Nucl. Mater.* 374 (2008) 281–285.
- [20] M.E. Broczkowski, D. Zagidulin, D.W. Shoesmith, The Role of Dissolved Hydrogen on the Corrosion/Dissolution of Spent Nuclear Fuel, in: Nuclear Energy and the Environment, American Chemical Society, Symposium, 2010, pp. 349–380.
- [21] P. Carbol, J. Cobos-Sabate, J.-P. Glatz, C. Ronchi, V. Rondinella, D.H. Wegen, T. Wiss, A. Loida, V. Metz, B. Kienzler, K. Spahiu, B. Grambow, J. Quinones, A. Martinez Esparza Valiente, The Effect of Dissolved Hydrogen on the Dissolution of ^{233}U -doped $\text{UO}_2(\text{s})$, High Burn-up Spent Fuel and MOX Fuel, Report TR-05-09, Swedish Nuclear Fuel and Waste Management Company, 2005.
- [22] M.E. Broczkowski, J.J. Noël, D.W. Shoesmith, The inhibiting effects of hydrogen on the corrosion of uranium dioxide under nuclear waste disposal conditions, *J. Nucl. Mater.* 346 (2005) 16–23.
- [23] M.E. Broczkowski, J.J. Noël, D.W. Shoesmith, The influence of dissolved hydrogen on the surface composition of doped uranium dioxide under aqueous corrosion conditions, *J. Electroanal. Chem.* 602 (2007) 8–16.
- [24] M.E. Broczkowski, P.G. Keech, J.J. Noël, D.W. Shoesmith, Corrosion of uranium dioxide containing simulated fission products in dilute hydrogen peroxide and dissolved hydrogen, *J. Electrochem. Soc.* 157 (2010) C275–C281.
- [25] M. Trummer, S. Nilsson, M. Jonsson, On the effects of fission product noble metal inclusions on the kinetics of radiation induced dissolution of spent nuclear fuel, *J. Nucl. Mater.* 378 (2008) 55–59.
- [26] D. Ofori, M.E. Broczkowski, H. He, K. O'Neil, O. Semenikhin, D.W. Shoesmith, The Influence of Various Factors on Fuel Corrosion under Nuclear Waste Disposal Conditions, Report TR-2011-20, Nuclear Waste Management Organization, 2011.
- [27] S. Nilsson, M. Jonsson, On the catalytic effects of $\text{Pd}(\text{s})$ on the reduction of UO_2^{2+} with H_2 in aqueous solution, *J. Nucl. Mater.* 374 (2008) 290–292.
- [28] M.E. Broczkowski, P.G. Keech, J.J. Noël, D.W. Shoesmith, The role of dissolved hydrogen on rare earth-doped uranium dioxide corrosion in the presence of hydrogen peroxide, *J. Electrochem. Soc.* 158 (2011) C439–C444.
- [29] S. Nilsson, M. Jonsson, On the catalytic effects of $\text{UO}_2(\text{s})$ and $\text{Pd}(\text{s})$ on the reaction between H_2O_2 and H_2 in aqueous solution, *J. Nucl. Mater.* 372 (2008) 160–163.
- [30] E. Ekeröth, M. Jonsson, T.E. Eriksen, K. Ljungqvist, S. Kovacs, I. Puigdomenech, Reduction of UO_2^{2+} by H_2 , *J. Nucl. Mater.* 334 (2004) 35–39.
- [31] F.J. Millero, S. Sotolongo, The oxidation of $\text{Fe}(\text{II})$ with H_2O_2 in seawater, *Geochim. Cosmochim. Acta* 53 (1989) 1867–1873.
- [32] F. Garisto, T. Kempe, P. Gierszewski, Technical Summary of the Safety Aspects of the Deep Geological Repository Concept for Used Nuclear Fuel, Report NWMO TR-2009-12, Nuclear Waste Management Organization, Toronto, ON, 2009.
- [33] D.G. Bennett, R. Gens, Overview of European concepts for high-level waste and spent fuel disposal with special reference waste container corrosion, *J. Nucl. Mater.* 379 (2008) 1–8.
- [34] J. Kaija, K. Rasilainen, R. Blomqvist, The use of selected safety indicators (concentrations, fluxes) in the assessment of radioactive waste disposal - Report 6, Report YST-114, Geological Survey of Finland - Nuclear Waste Disposal Research, 2003.
- [35] H. Christensen, R. Forsyth, R. Lundqvist, L.O. Werme, Radiation Induced Dissolution of UO_2 , Report NS-90/85, Studsvik Energiteknik AB, Nyköping, Sweden, 1990.
- [36] P. Diaz-Arocas, J. Quinones, C. Maffiotte, J. Serrano, J. Garcia, J.R. Almazan, *Mater. Res. Soc. Symp. Proc.* 353 (1995) 641–646.
- [37] S. Sunder, N.H. Miller, D.W. Shoesmith, Corrosion of uranium dioxide in hydrogen peroxide solutions, *Corros. Sci.* 46 (2004) 1095–1111.
- [38] J. de Pablo, I. Casas, F. Clarens, F. El Amrani, M. Rovira, The effect of hydrogen peroxide concentration on the oxidative dissolution of unirradiated uranium dioxide, *Mater. Res. Soc. Symp. Proc.* 663 (2001) 409–426.
- [39] M. Jonsson, E. Ekeröth, O. Roth, *Mater. Res. Soc. Symp. Proc.* 807 (2004) 77.
- [40] T.E. Eriksen, D.W. Shoesmith, M. Jonsson, Radiation induced dissolution of UO_2 based nuclear fuel – a critical review of predictive modelling approaches, *J. Nucl. Mater.* 420 (2012) 409–423.
- [41] S. Sunder, Calculation of radiation dose rates in a water layer in contact with used CANDU UO_2 fuel, *Nucl. Tech.* 122 (1998) 211–221.
- [42] F. Garisto, J. Avis, N. Calder, A. D'Adrea, P. Gierszewski, C. Kitson, T. Melnyk, K. Wei, L. Wojciechowski, Third Case Study – Defective Container Scenario, Report O6219-REP-01200-10126-R00, Ontario Power Generation, Toronto, ON, 2004.
- [43] A. Poulesquen, C. Jégou, S. Peugot, Determination of alpha dose rate profile at the UO_2 /water interface, in: P. Van Iseghem (Ed.) Scientific Basis for Nuclear Waste Management XXIX, Material Research Society (*Mater. Res. Soc. Symp. Proc.* 932), Warrendale, PA, 2006, pp. 505–512.
- [44] W. Xu, K. Daub, X. Zhang, J.J. Noël, D.W. Shoesmith, J.C. Wren, Oxide formation and conversion on carbon steel in mildly basic solutions, *Electrochim. Acta* 54 (2009) 5727–5738.
- [45] R. Wiebe, V.L. Gaddy, J. Conrad Heins, Solubility of Hydrogen in Water at 25°C from 25 to 1000 Atmospheres, *Indus. Eng. Chem.* 24 (1932) 823–825.
- [46] T.E. Crozier, S. Yamamoto, Solubility of hydrogen in water, seawater, and NaCl solutions, *J. Chem. Eng. Data* 19 (1974) 242–244.
- [47] C.F. Baes, R.E. Mesmer, *The Hydrolysis of Cations*, Jon Wiley and Sons, New York, 1976.